

Quantum dynamics of Bose-Einstein condensates in tilted and driven bichromatic optical lattices

D. Witthaut,^{1,2,3} F. Trimborn,^{4,3} V. Kegel,³ and H. J. Korsch³

¹*Network Dynamics Group, Max-Planck Institute for Dynamics and Self-Organization, D-37073 Göttingen, Germany*

²*QUANTOP, The Niels Bohr Institute, University of Copenhagen, DK-2100 Copenhagen, Denmark*

³*Fachbereich Physik, TU Kaiserslautern, D-67663 Kaiserslautern, Germany*

⁴*Institut für theoretische Physik, Leibniz Universität Hannover, D-30167 Hannover, Germany*

(Dated: December 15, 2010)

We study the dynamics of Bose-Einstein condensates in tilted and driven optical superlattices. For a bichromatic lattice, each Bloch band split up into two minibands such that the dynamics is governed by the interplay of Bloch oscillations and transitions between the bands. Thus, bichromatic potentials provide an excellent model system for the study of nonlinear Landau-Zener tunneling and allow for a variety of applications in matter wave interferometry and quantum metrology. In the present paper we investigate the coherent dynamics of an interacting Bose-Einstein condensate as well as its stability. Different mechanisms of instability are discussed, which lead to a rapid depletion of the condensate.

PACS numbers: 03.75.Lm, 03.65.Sq

I. INTRODUCTION

Despite its apparent simplicity, the dynamics of quantum particles in periodic structures is full of surprises. Contrary to our intuition, a weak external field inhibits quantum transport in a periodic potential in favor of the celebrated Bloch oscillations [1, 2]. For stronger fields a directed motion is re-introduced by repeated Landau-Zener transitions to higher Bloch bands [3–6]. One of the most interesting physical systems to explore the dynamics in periodic potentials are Bose-Einstein condensates (BEC) in optical lattices, allowing an in situ detection of the atoms [7, 8]. In recent years it became possible to realize periodic potentials with almost arbitrary shapes and an astonishing precision. Bichromatic lattices have been implemented by superimposing two incoherent optical lattices [9, 10], or by combining optical potentials based on virtual two-photon and four-photon processes [11–15]. These superlattices allow to engineer the Bloch band structure of the system by tuning few experimental parameters.

The dynamics of a BEC in a tilted optical lattice, and especially the Landau-Zener tunneling between Bloch bands, is strongly modified by the inter-atomic interactions. While the fundamental problem of Landau-Zener tunneling between two levels was solved as early as 1932 independently by Landau, Zener, Majorana and Stückelberg [3–6], a generalization of these results to interacting many-particle systems remains an open question up to today. The possibility to investigate Landau-Zener tunneling of a BEC in situ in a well controllable laboratory experiment has thus attracted much interest in recent years. A distinguished result of these studies was that strong interactions in a BEC lead to a breakdown of adiabaticity and instability even in the limit of very slow parameter variations. This phenomenon was first predicted theoretically within a mean-field approximation [16–19] and demonstrated for a BEC in an accel-

erated optical lattice shortly afterwards [20–24]. Later, it was shown theoretically that the breakdown of adiabaticity results from the occurrence of diabatic level crossings in the many-body spectrum [25–27].

In a bichromatic optical lattice, it is possible to tune the energy gap between the minibands via the relative phase of the two lattices and thus to control Landau-Zener tunneling as shown in [12]. Furthermore, the band structure can be engineered such that the BEC is confined to the two lowest minibands and cannot be lost by repeated tunneling to higher excited bands, such that one can even observe repeated Landau-Zener tunneling events [15, 28, 29]. In addition, Landau-Zener tunneling can be used as a coherent beam splitter for atomic matter waves, which enables a variety of possible applications in matter wave interferometry and quantum metrology [15].

In the present paper we will provide a thorough theoretical analysis of nonlinear Landau-Zener tunneling in bichromatic optical lattices with a focus on the onset of dynamical instability and depletion of the condensate. Furthermore, we study Bloch-Zener oscillations, the coherent superposition of Bloch oscillations and Landau-Zener tunneling, and the dynamics in driven lattices, where transitions between the minibands are caused by the periodic driving instead of a static field. In the latter case, the dynamics of a BEC is governed by the interference of two matter waves with the same quasi momentum and opposite group velocity. This gives rise to an oscillatory motion which can be viewed as a simple quantum simulation of the *Zitterbewegung* of a relativistic Dirac spinor.

We focus on a bichromatic optical lattice with an alternating depth of the lattice wells. The many-body dynamics in such an optical lattice is described by the Bose-

Hubbard type hamiltonian [30]

$$H = -J \sum_{n=1}^{M-1} (\hat{a}_{n+1}^\dagger \hat{a}_n + \hat{a}_n^\dagger \hat{a}_{n+1}) + \frac{U}{2} \sum_{n=1}^M \hat{a}_n^{\dagger 2} \hat{a}_n^2 + \sum_{n=1}^M \left(\frac{\delta}{2} (-1)^n + Fn \right) \hat{a}_n^\dagger \hat{a}_n, \quad (1)$$

where \hat{a}_n and \hat{a}_n^\dagger are the bosonic annihilation and creation operators, respectively. The parameter J denotes the tunneling rate between the wells, U is the interaction strength and F the strength of the static external field which accelerates the atoms. The parameter $\delta \geq 0$ is the difference of the on-site energies between adjacent wells. It is directly proportional to the intensity of the double-periodic optical lattice. In the following we set $J = 1$ in all simulations, i.e. we measure all energies in units of the tunneling matrix element J .

One of the main objectives of the present paper is a careful analysis of how the interactions affect the coherent dynamics of a BEC in a bichromatic lattice and how they possibly lead to instabilities of the condensate. Throughout the paper we thus assume that the system is initially prepared as a pure BEC with N particles:

$$|\Psi(0)\rangle = \frac{1}{\sqrt{N!}} \left(\sum_n \psi_n \hat{a}_n^\dagger \right)^N |0\rangle. \quad (2)$$

As long as the quantum state remains close to a pure BEC, the dynamics is well described within a mean-field approximation. The dynamics of the condensate wave function is then given by the discrete nonlinear Schrödinger equation (DNLS) [8]

$$i\dot{\psi}_n = -J(\psi_{n+1} + \psi_{n-1}) + \left[\frac{(-1)^n \delta}{2} + Fn + UN|\psi_n|^2 \right] \psi_n. \quad (3)$$

However, dynamical instabilities lead to a depletion of the condensate such that the mean-field approximation is no longer applicable. In order to simulate the dynamics beyond mean-field we use the Bogoliubov backreaction (BBR) method which also gives a quantitative prediction for the depletion of the condensate [31–33].

II. BLOCH STATES AND BANDS

Bloch states are the simultaneous eigenstates of the field-free Hamiltonian and a translation over *two* lattice sites. The dynamics of a BEC can be understood to a large extent from the properties of linear and non-linear Bloch states, including the depletion of the condensate. In the following we thus give a detailed analysis of the Bloch states and their stability.

A. Single-particle Bloch states

In the simplest case of a single atom, where interactions are obviously irrelevant, the Bloch bands are easily

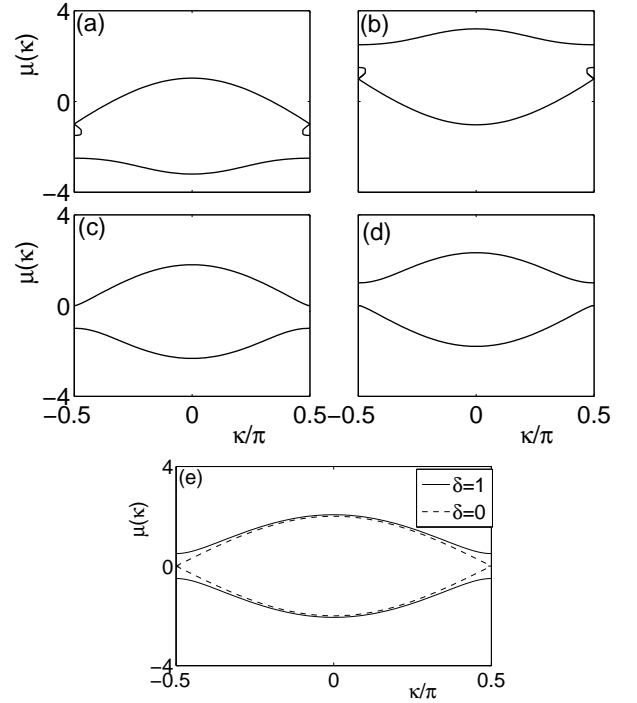


FIG. 1: Nonlinear Bloch bands in a bichromatic optical lattice with $\delta = 1$ for $g = -2$ (a), $g = +2$ (b), $g = -0.5$ (c) and $g = +0.5$ (d). Linear Bloch bands ($g = 0$) are shown in (e) for $\delta = 1$ (solid line) and $\delta = 0$ (dashed line) for comparison.

calculated as [28]

$$E_\alpha(\kappa) = \frac{(-1)^{\alpha+1}}{2} \sqrt{\delta^2 + 4J^2 \cos^2(\kappa)}, \quad (4)$$

where $\alpha = 0, 1$ labels the two minibands and $\kappa \in [-\pi/2, +\pi/2]$ denotes the quasimomentum. The band gap between the two minibands is directly given by the parameter δ . The corresponding Bloch states are given by $|\chi_{\alpha,\kappa}\rangle = \hat{b}_{\alpha,\kappa}^\dagger |0\rangle$, where

$$\begin{aligned} \hat{b}_{0,\kappa} &= \frac{1}{\sqrt{N_\kappa}} \sum_n u_\kappa e^{i2n\kappa} \hat{a}_{2n} + v_\kappa e^{i(2n+1)\kappa} \hat{a}_{2n+1} \\ \hat{b}_{1,\kappa} &= \frac{1}{\sqrt{N_\kappa}} \sum_n v_\kappa e^{i2n\kappa} \hat{a}_{2n} - u_\kappa e^{i(2n+1)\kappa} \hat{a}_{2n+1} \end{aligned} \quad (5)$$

and

$$\begin{aligned} u_\kappa &= 4J \cos(\kappa) \\ v_\kappa &= \delta + \sqrt{\delta^2 + 4J^2 + \cos^2(\kappa)}, \end{aligned}$$

$N_\kappa = \pi(u_\kappa^2 + v_\kappa^2)$ being a normalization constant.

B. Nonlinear Bloch bands

Also in the mean-field approximation one can analytically calculate the 'nonlinear' Bloch states, which are

defined as stationary states of the DNLSE

$$\mu\phi_n = -J(\phi_{n+1} + \phi_{n-1}) + UN|\phi_n|^2\phi + (-1)^n \frac{\delta}{2}\phi_n, \quad (6)$$

with the translation symmetry $\phi_{n+2} = e^{2i\kappa}\phi_n$. Making the ansatz

$$\phi_n \sim \begin{cases} u_\kappa e^{i\kappa n} & n \text{ even} \\ v_\kappa e^{i\kappa n} & n \text{ odd}, \end{cases} \quad (7)$$

one finds that the coefficients u_κ, v_κ are determined by the two-mode DNLSE

$$\begin{pmatrix} \delta/2 + g|u_\kappa|^2 & -2J\cos(\kappa) \\ -2J\cos(\kappa) & -\delta/2 + g|v_\kappa|^2 \end{pmatrix} \begin{pmatrix} u_\kappa \\ v_\kappa \end{pmatrix} = \mu \begin{pmatrix} u_\kappa \\ v_\kappa \end{pmatrix}. \quad (8)$$

Using the normalization $|u_\kappa|^2 + |v_\kappa|^2 = 1$, the effective coupling constant is given by $g = 2U\rho$, ρ being the average particle density. Examples of nonlinear Bloch bands are shown in Fig. 1. One observes that the bands become strongly asymmetric – for a repulsive nonlinearity $g > 0$ the curvature of the ground band increases while the curvature of the excited band decrease and vice versa for an attractive nonlinearity $g < 0$. For strong nonlinearities novel stationary states appear at the band edge $\kappa = \pm\pi/2$, forming the so-called looped Bloch bands [34, 35]. A quantitative analysis shows that DNLSE (8) admits four solutions if [18]

$$g^{2/3} > \delta^{2/3} + |2J\cos(\kappa)|^{2/3}. \quad (9)$$

Thus the critical nonlinearity for the existence of looped levels is directly linked to the band gap δ . The deformation of the Bloch bands has significant consequences for the dynamics which will be discussed in detail in Sec. III A. An adiabatic dynamics is hindered by a sharpening of the levels and becomes completely impossible as soon as the loops form.

C. Stability analysis

The nonlinear Bloch states calculated in the preceding section are stationary states of the DNLSE (3). However, they can become dynamically unstable due to the nonlinear interaction term, which also indicates a rapid depletion of the BEC. In order to determine the stability properties of a Bloch state (7), we add a small perturbation with quasimomentum q :

$$\begin{aligned} \psi_n(t) &= e^{-i\mu t}\phi_n \\ &+ \begin{cases} e^{i(\kappa n - \mu t)}(\xi_{0,\kappa}e^{iqn} + \zeta_{0,\kappa}^*e^{-iqn}) & n \text{ even} \\ e^{i(\kappa n - \mu t)}(\xi_{1,\kappa}e^{iqn} + \zeta_{1,\kappa}^*e^{-iqn}) & n \text{ odd} \end{cases} \end{aligned} \quad (10)$$

and analyze the consequences for the energy and the dynamics of the condensate. If every perturbation increases the total energy given by the Gross-Pitaevskii energy

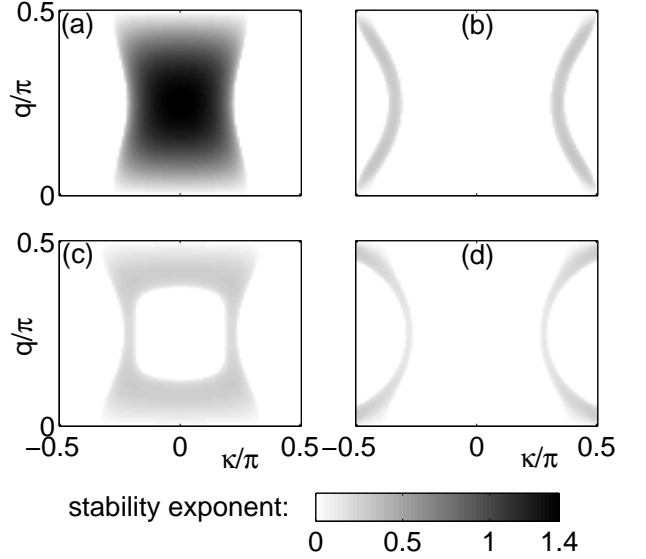


FIG. 2: Stability map for a nonlinear Bloch state with quasimomentum κ in the ground band for $\delta = 1$ and $g = -2$ (a), $g = +2$ (b), $g = -0.5$ (c) and $g = +0.5$ (d). The gray scale map shows the stability exponent, i.e. the growth rate of a perturbation with quasimomentum q . Dynamical instability leads to a depletion of the condensate if the stability exponent is non-zero for at least one value of q .

functional

$$\begin{aligned} E &= -J \sum_n \psi_{n+1}^* \psi_n + \psi_n^* \psi_{n+1} + \frac{UN}{2} \sum_n |\psi_n|^4 \\ &+ \frac{\delta}{2} \sum_n (-1)^2 |\psi_n|^2, \end{aligned} \quad (11)$$

then the Bloch state represents a local energy minimum and thus a stable superflow. Otherwise a perturbation may lower the energy and the Bloch state suffers a Landau instability. In the present paper we are more concerned with the dynamical instability of a Bloch state, which occurs if a perturbation grows exponentially, as this indicates a rapid depletion of the condensate mode [36–39]. Note that dynamical instability always indicates energetical instability but not vice versa [35].

In order to determine the energetical stability we substitute the ansatz (10) into the Gross-Pitaevskii energy functional (11) and expand it up to second order in the perturbation. The variation of the energy is then given by

$$\delta E = \int dq \Xi_\kappa^\dagger L_{\text{en}}(\kappa, q) \Xi_\kappa \quad (12)$$

with the matrix

$$L_{\text{en}}(\kappa, q) = \begin{pmatrix} H(\kappa + q) & gV \\ gV^* & H(\kappa - q) \end{pmatrix}. \quad (13)$$

Here we have introduced the abbreviations

$$H(k) = \begin{pmatrix} \frac{\delta}{2} + 2g|u|^2 - \mu & -2J \cos(k) \\ -2J \cos(k) & -\frac{\delta}{2} + 2g|v|^2 - \mu \end{pmatrix},$$

$$V = \begin{pmatrix} u^2 & 0 \\ 0 & v^2 \end{pmatrix} \quad \text{and}$$

$$\Xi_\kappa = (\xi_{0,\kappa}, \xi_{1,\kappa}, \zeta_{0,\kappa}, \zeta_{1,\kappa})^T. \quad (14)$$

The Bloch state represents a stable energy minimum if δE is positive for any perturbation, i.e. if the matrix $L_{\text{en}}(\kappa, q)$ is positive definite for every q .

The dynamical stability properties are found by substituting the ansatz (10) into the DNLS (3). In first order, the perturbation evolves according to the Bogoliubov-de Gennes equation

$$i \frac{d}{dt} \Xi_\kappa = L_{\text{BdG}}(\kappa, q) \Xi_\kappa \quad (15)$$

with

$$L_{\text{BdG}}(\kappa, q) = \sigma_z L_{\text{en}}(\kappa, q) = \begin{pmatrix} H(\kappa + q) & gV \\ -gV^* & -H(\kappa - q) \end{pmatrix}. \quad (16)$$

A dynamical instability occurs if a perturbation grows exponentially, i.e. if there is any q for which the eigenvalues of the matrix $L_{\text{BdG}}(\kappa, q)$ are not purely real.

The dynamical stability for the Bloch states in the ground band is depicted in Fig. 2 for the same parameters as in Fig. 1. A grey scale map shows the stability exponent, i.e. the maximum imaginary part of the eigenvalues of the Bogoliubov-de Gennes matrix $L_{\text{BdG}}(\kappa, q)$ in dependence of κ and q . This imaginary part indicates the growth rate of a perturbation with wavenumber q and thus also the depletion rate of the condensate. A Bloch state with quasimomentum κ is dynamically stable only if the growth rate is zero for all values of q . One observes that two different kinds of dynamical instability exist in a bichromatic lattice. In the attractive case $g < 0$, the Bloch states in the center of the Brillouin zone become strongly unstable already for a quite modest nonlinearity. Thus we face the surprising conclusion that an attractive interaction on the one hand flattens the ground band and thus facilitates an adiabatic evolution, but on the other hand leads to instability. On the contrary, a strong repulsive nonlinearity is required to introduce a weak dynamic instability at the edge of the Brillouin zone, which is associated with the occurrence of looped Bloch bands. Thus one can infer that a significant depletion takes place only for a much stronger interaction than in the attractive case and that it sets in at the edge of the Brillouin zone around $\kappa = \pi/2$.

III. DYNAMICS

The dynamics of a BEC in a bichromatic optical lattice is governed by the interplay of the intraband dynamics

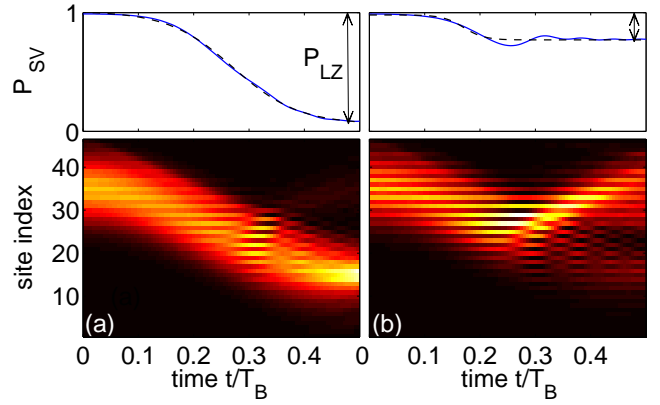


FIG. 3: (Color online) Many-particle Landau-Zener tunneling between two minibands with band gap $\delta = 0.2$ (a) and $\delta = 1$ (b). The dynamics has been calculated with the BBR method for the parameters $J = 1$, $F = 0.2$, $UN = 2$ and $N = 100$ particles. The upper panels show the survival probability (18) in the upper half of the lattice (solid line).

and the transitions between the two minibands. A static force can be introduced by gravity [20], magnetic field gradients [41], or by an acceleration of the complete lattice (see [8] and references therein). This force accelerated the atoms until they are finally Bragg reflected, leading to the celebrated Bloch oscillations [1, 2, 13]. In addition, this force induces Landau-Zener tunneling between the minibands [12], which will be investigated in detail in the following. In a bichromatic lattice one can control the tunneling rate to a large extent by tuning the lattice parameters [11]. On longer timescale repeated Landau-Zener tunneling takes place, which leads to a complex dynamics due to the interference effects of atoms in the two minibands [15, 28, 29]. Finally, we will extend our analysis to the case where transitions are not driven by an external field but by a periodic driving.

In order to simulate the dynamics beyond the mean-field approximation and to describe the depletion of the condensate we use the Bogoliubov backreaction (BBR) method introduced in [31–33]. In this approach one takes into account two- and four point functions and truncates all higher order correlation functions to obtain a closed set of evolution equations. The BBR method has proven its worth to predict the features of the many-body quantum state, especially the depletion of the condensate mode, avoiding the common problems of the Hartree-Fock-Bogoliubov approximation [31–33]. In particular the nature of the many-body quantum state is indicated by the reduced single-particle density matrix (SPDM) [7, 31–33]

$$\sigma_{j,m} = \frac{1}{N} \langle \hat{a}_j^\dagger \hat{a}_m \rangle. \quad (17)$$

The leading eigenvalue of this matrix, λ_0 , gives the fraction of atoms in the condensate mode. Consequently, the non-condensed fraction is given by $1 - \lambda_0$.

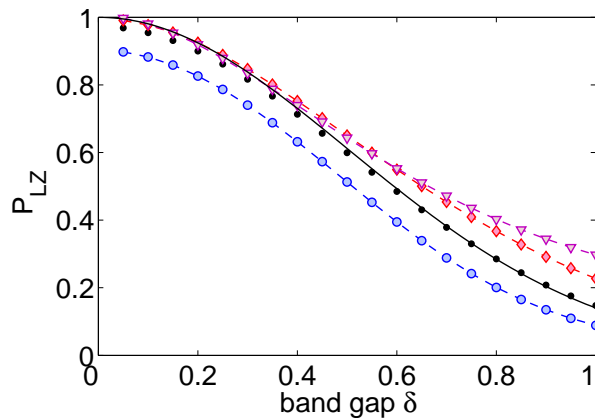


FIG. 4: (Color online) Landau-Zener tunneling probability P_{LZ} between two minibands as a function of the band gap δ for $UN = -2$ (\circ), $UN = 0$ (\cdot), $UN = +2$ (\diamond) and $UN = +4$ (∇) and $N = 100$ particles. The solid line shows the analytic approximation (19) for the linear case. Dashed lines are plotted to guide the eye.

A. Nonlinear Zener tunneling

To begin with, we explore the basic features of the dynamics in a bichromatic lattice subject to a static external field, Bloch oscillations and Landau-Zener tunneling, for the weakly interacting case. We assume that the initial state is a pure BEC (2) in the ground Bloch band with $\kappa = 0$ weighted by a Gaussian envelope $\psi_n(0) \sim \phi_n \exp(-(n - n_0)^2/4\sigma^2)$ with a width of $\sigma = 5$ sites centered around the site $n_0 = 35$. In the forthcoming examples we choose the total particle number to be $N = 100$ located in a lattice with $M = 46$ sites and $F = 0.2$, unless otherwise stated. A weak nonlinearity induces a reversible dephasing, which damps Bloch oscillations [39–41], and, of course, alters the Landau-Zener tunneling rate between the two minibands.

Figure 3 shows two examples of the many-body dynamics starting from the initial state (2) for a weak repulsive interaction, $UN = 2$, and two different values of the band gap δ . The figures show the evolution of the density $\langle \hat{n}_j(t) \rangle$, $j = 1, \dots, M$ in false color. Here and in the following, we take the Bloch time $T_B = 2\pi/F$ of the single-periodic lattice ($\delta = 0$) as the reference time scale. One observes that the BEC is first accelerated by the external field F until it reaches the edge of the Brillouin zone at $T = T_B/4$. If the band gap δ is large (Fig. 3 (b)), the BEC matter wave stays in the ground miniband and performs Bloch oscillations with a period of $T_B/2$. In contrast, if the gap is small, the matter wave tunnels to the excited miniband and performs Bloch oscillations with the full period T_B (Fig. 3 (a)). At time $t = T_B/2$ it is located at the turning point of the Bloch oscillations. For intermediate values of the band gap, only a fraction of the condensate tunnels to the excited miniband and the wavepacket splits.

For a further quantitative analysis of the Landau-Zener

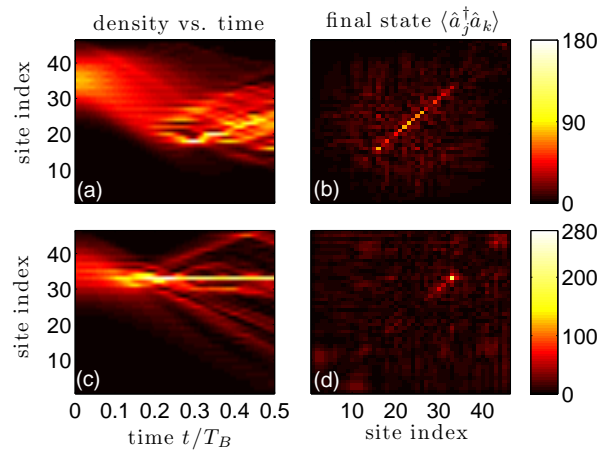


FIG. 5: (Color online) Unstable dynamics in a tilted bichromatic optical lattice for strong interactions $UN = +20$ (a,b) and $UN = -10$ (c,d). The left panels (a,c) show the evolution of the density and the right-panels (b,d) show the magnitude of the scaled SPDM $N|\sigma_{j,k}| = |\langle \hat{a}_j^\dagger \hat{a}_k \rangle|$ at $t = T_B/2$ in a colormap plot. The remaining parameters are $\delta = 0.2$ and $N = 1000$.

tunneling rate we estimate the survival probability in the ground miniband by the number of atoms remaining in the upper half of the lattice:

$$P_{SV}(t) = \frac{1}{N} \sum_{j=24}^{46} \langle \hat{n}_j(t) \rangle. \quad (18)$$

The Landau-Zener tunneling probability to the excited band is then given by $P_{LZ} := 1 - P_{SV}(T_B/2)$. The time dependence of the survival probability (18) is shown in the upper panels of Fig. 3 together with P_{LZ} .

Figure 4 shows the Landau-Zener tunneling probability P_{LZ} in dependence of the band gap δ for different values of the interaction strength UN . In the linear case, $UN = 0$, one can approximate the avoided crossing of the two minibands at the edge of the Brillouin zone by an effective two-level model which yields the following approximation for the Landau-Zener probability [28]:

$$P_{LZ}^{(0)} \approx \exp\left(-\frac{\pi\delta^2}{8JF}\right). \quad (19)$$

This approximation shows an excellent agreement with the numerical results shown in Fig. 4. In the weakly nonlinear case one observes an increase of the Landau-Zener tunneling rate P_{LZ} for a repulsive nonlinearity $U > 0$ and a decrease for an attractive nonlinearity $U < 0$, which has also been demonstrated experimentally [21]. This effect can be understood from the structure of the nonlinear Bloch states introduced above. With increasing interaction strength, the nonlinear Bloch bands $\mu(\kappa)$ become strongly asymmetric as shown in Fig. 1. For $UN < 0$, the ground band is flattened so that adiabaticity is facilitated and P_{LZ} decreases, while the excited band is sharpened.

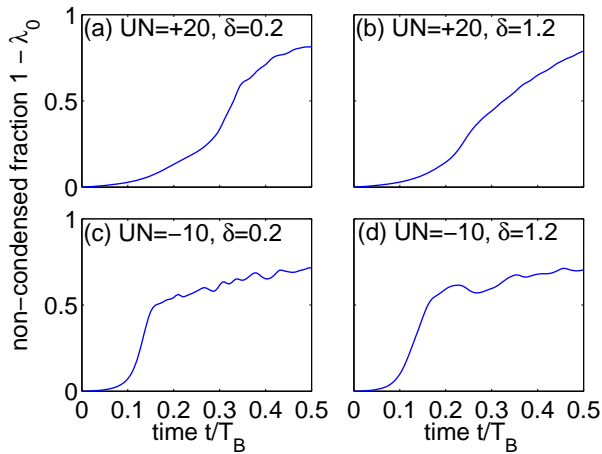


FIG. 6: (Color online) Depletion of the condensate during nonlinear Landau-Zener tunneling. Temporal growth of the non-condensed fraction $1 - \lambda_0$ for a strong repulsive interaction $UN = +20$ (a,b) and an attractive interaction $UN = -10$ (c,d). The remaining parameters are $\delta = 0.2$ (a,c) and $\delta = 1.2$ (b,d), respectively, and $N = 1000$.

The inverse effect is found for $UN > 0$ such that P_{LZ} increases. If the nonlinearity UN exceeds a critical value, a Bloch state at the edge of a band bifurcates to a looped structure, which prevents an adiabatic evolution even for very small values of F .

B. Depletion of the condensate

Strong inter-atomic interactions alter the dynamics of the BEC completely. Examples are shown in Fig. 5 for a repulsive (a,b) and an attractive (c,d) interaction, respectively. One observes that the familiar Bloch oscillation pattern is significantly disturbed, especially in the case of attractive interactions. In the repulsive case, the atoms are distributed over several lattice sites, but the phase coherence between these sites is lost almost completely. This is indicated by a strong suppression of the non-diagonal parts of the SPDM as shown in Fig. 5 (b). A strong attractive nonlinearity leads to a collapse of the condensate. Figure 5 (c) shows that the atoms are strongly focussed to a single lattice site at $t \approx 0.15 T_B$. Afterwards, a fraction of the atoms 'explodes' from the focus and the condensate mode is rapidly depleted.

To further analyze the different mechanisms of instability due to repulsive and attractive interactions we calculate how the condensate is depleted. Figure 6 shows the time evolution of the non-condensed fraction $1 - \lambda_0$ for a strong repulsive ($UN = +20$) and a strong attractive nonlinearity ($UN = -10$), respectively. In the attractive case, instability sets in much earlier and takes place on a very short time scale. This difference can be explained by the results of a linear stability analysis as discussed in Sec. II C. In the repulsive case the onset of dynamical instability can be associated with the emergence of

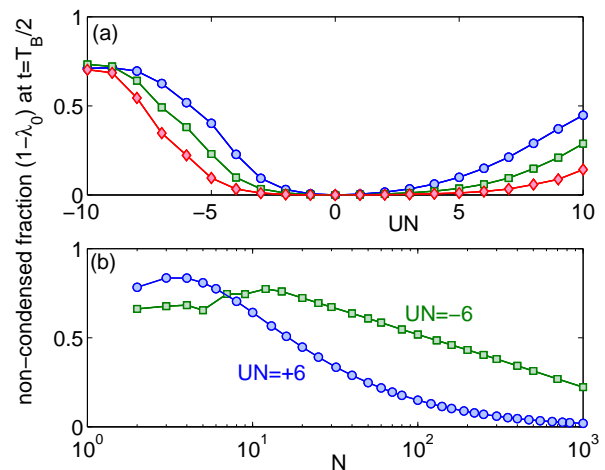


FIG. 7: (Color online) The non-condensed fraction $1 - \lambda_0$ at time $t = T_B/2$ as a function of (a) the interaction strength UN for $N = 100$ (\circ), $N = 300$ (\square) and $N = 1000$ (\diamond) and (b) as a function of the particle number N for a fixed interaction strength $UN = +6$ (\circ) and $UN = -6$ (\square). Solid lines are drawn to guide the eye.

looped Bloch bands. The condensate becomes dynamically unstable at the edge of the Brillouin zone where the loops emerge. In contrast, already modest attractive interactions lead to a dynamic instability at the center of the Brillouin zone (cf. Fig 2) such that the depletion of the condensate sets in immediately.

A quantitative analysis of the depletion of the condensate is provided in Fig. 7, where we have plotted the non-condensed fraction at $t = T_B/2$ as a function of the interaction strength UN in (a) and the particle number N for a fixed value of the interaction strength $UN = \pm 6$ in (b). Figure 7 (a) clearly shows the qualitative difference between an attractive and a repulsive interaction. In the first case, one observes a rapid increase of the non-condensed fraction when the interaction strength exceeds the critical value for the onset of a dynamical instability. For a repulsive interaction, however, the dynamics is rather stable so that the non-condensed fraction remains small for all values of $|UN| < 10$ shown in the figure. The non-condensed fraction decreases with the particle number and tends to zero in the mean-field limit $N \rightarrow \infty$. However, the speed of convergence depends crucially on the stability of the dynamics as shown in Fig. 7 (b). In the repulsive case, $UN = +6$, the dynamics is stable and thus convergence is fast. The non-condensed fraction decreases rapidly with increasing particle number such that the mean-field description by the DNLSE is valid already for quite small values of the particle number. On the contrary, the convergence is logarithmically slow for $UN = -6$ due to the dynamical instability. A different approach to a classical instability causing depletion is provided by generalized mean-field descriptions [36–38].

C. Bloch-Zener oscillations

On a longer timescale, the dynamics of a BEC in a tilted optical lattice is governed by the interference of Bloch oscillations and Zener tunneling between the Bloch bands [28, 29]. Figure 8 (b) shows an example of the dynamics of the atomic density for $\delta = 0.5$. The condensate wave packet is coherently split by Landau-Zener tunneling between the two minibands at $t = T_B/4$ and recombined again at $t = 3T_B/4$, thus realizing an effective matter wave Mach-Zehnder interferometer. The splitting ratio of this interferometer, which is given by the Landau-Zener tunneling rate (19), is easily tunable by changing the band gap δ .

For very small and for very large values of δ , the condensate occupies only one miniband – it remains in the ground band for large δ and tunnels completely to the other miniband for small δ as shown in Fig. 8 (c). In both cases the condensate shows simple Bloch oscillations and returns back to its initial state at $t = T_B$. For intermediate values of δ , the condensate is split into two parts at $t = T_B/4$. The further dynamics and especially the occupation of the two minibands is governed by the interference of the two possible paths. For the given parameters, about one half of the population is still localized in the excited miniband at $t = T_B = 2\pi/F$. In this parameter range, the dynamics is very sensitive even to small nonlinearities as shown in Fig. 8 (d). The survival probability at $t = T_B$ differs significantly for $UN = -1$ and $UN = +1$, although the nonlinearity is still comparatively weak.

For the given interaction strength $|U| \leq 1$, the splitting and also the recombination of the condensate is fully coherent; the fraction of non-condensed atoms is less than 0.4% at $t = 2T_B$ as shown in Fig. 8 (a). A significant depletion of the condensate is observed only for stronger nonlinearities; for instance the non-condensed fraction at $t = 2T_B$ exceeds 10% for $UN \gtrsim 5$.

This example demonstrates the possible use of Landau-Zener tunneling and Bloch-Zener oscillations in quantum metrology. These tools can be used, for instance, to directly measure the band structure of a bichromatic potential as demonstrated in [15]. This is a unique feature of bichromatic optical lattices. In a simple periodic potential, a matter wave will be accelerated further towards $-\infty$ after it has escaped from the ground band, such that no interference can be observed.

D. Coupling of bands by a periodic driving

Previously, we have discussed the effects of Zener tunneling between the two minibands induced by the external field F . A coupling of the bands can also be introduced in the field free case by a periodic driving of the system parameters. This has the advantage that the quasi momentum κ is conserved such that a different regime of the dynamics can be explored.

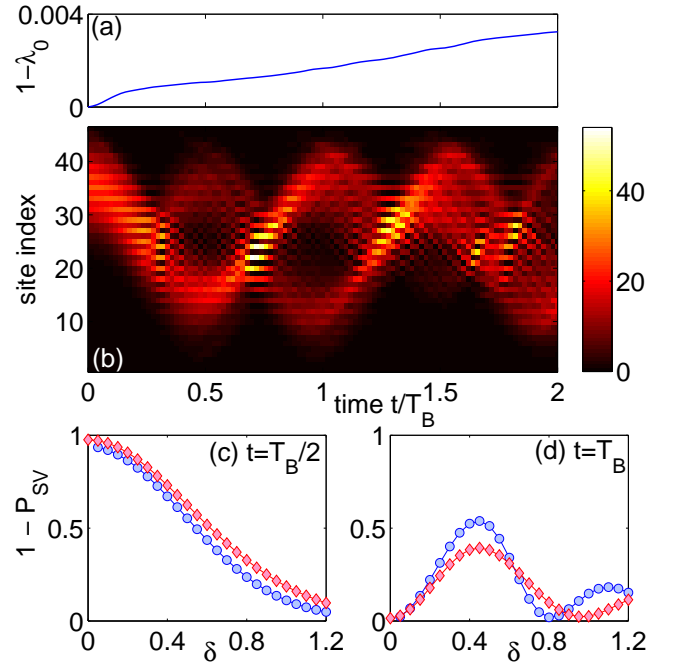


FIG. 8: (Color online) Bloch-Zener oscillations of a BEC with $N = 300$ atoms in a tilted bichromatic lattice. (a) Non-condensed fraction $1 - \lambda_0$ for $\delta = 0.5$ and $UN = 1$. (b) Atomic density in real space for $\delta = 0.5$ and $UN = 1$. (c,d) Survival probability (18) in the upper half of the lattice after $t = T_B/2$ and $t = T_B$, respectively, for $UN = -1$ (o) and $UN = +1$ (◊).

Here we consider a BEC initially prepared in the ground miniband with a well defined quasimomentum κ . The strength of the double-periodic optical lattice is varied in time to realize a harmonic driving of the energy offset

$$\delta(t) = \delta_0 + \delta_1 \cos(\omega t). \quad (20)$$

This driving induces transitions between the two minibands if the frequency is chosen to be resonant with the band gap, $\omega = E_1(\kappa, \delta_0) - E_0(\kappa, \delta_0)$. In the following example we set $\delta_0 = 0.4$, $\delta_1 = 0.2$ and $U = 0$. The initial state is assumed to be pure BEC with momentum $\kappa = 0.1\pi$, weighted by a Gaussian envelope with $\sigma = 10$. The resulting dynamics is shown in Fig. 9 in real (left) and momentum space (right). One clearly observes the transitions between the two minibands, while the quasimomentum of the BEC is conserved (panel (b)). A further quantitative analysis of this effect is provided in panel (d), where the occupation of the two minibands $p_{0,1}$ is plotted. The oscillation between the bands has remarkable consequences for the real-space dynamics of the BEC shown on the left-hand side of the figure. As the two minibands have opposite curvature, a transition between the bands reverses the group velocity of the matter wave. This leads to an oscillatory motion of the mean position, which can be understood as a quantum simulation of the *Zitterbewegung* of a Dirac spinor. This relativistic

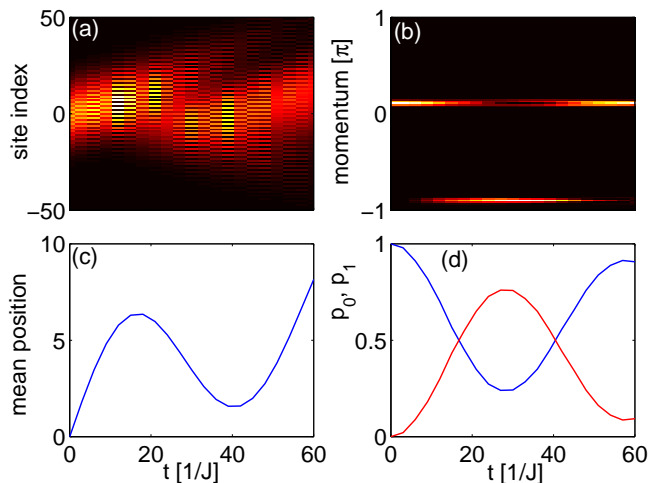


FIG. 9: (Color online) Quantum dynamics of BEC in a bichromatic lattice with periodic driving $\delta(t)$ and $F = 0$. (a,b) Atomic density in real and momentum space, respectively. (c) Position expectation value $\sum_j j \langle \hat{n}_j \rangle / N$. (d) Occupation of the two minibands p_0 (blue) and p_1 (red).

effect results from the interference of particle and anti-particle contributions moving to opposite directions. In the discussed quantum simulator, the two minibands thus play the role of particle and anti-particle contributions, respectively. Similar effects were recently predicted for optical waveguide arrays [42, 43].

IV. CONCLUSION AND OUTLOOK

We have discussed the dynamics of a Bose-Einstein condensate in a bichromatic optical lattice. In such a lattice, the ground Bloch band splits up into two minibands with a controllable band gap. Hence, they are ideally suited to study the complex quantum dynamics resulting from the interplay of the intraband dynamics and transition between the minibands.

The basic dynamics of a BEC in an optical lattice can be inferred from the band structure of the system. Within the tight-binding approximation, one can readily calculate the linear as well as the nonlinear Bloch states. In particular, this treatment yields an explicit expression for the critical interaction strength for the occurrence of looped Bloch bands, which leads to a breakdown of

adiabatic motion. The stability properties of the Bloch states have been analyzed in detail by the Bogoliubov-de Gennes approach.

The dynamics of a BEC was simulated using the Bogoliubov backreaction method which also provides a quantitative estimate for the depletion of the condensate. The Landau-Zener tunneling of a BEC between minibands in a tilted or accelerated bichromatic lattice has been investigated in detail. For weak interactions, the condensate remains essentially intact, whereas the Landau-Zener tunneling process is strongly affected. Repulsive interactions increase the tunneling rate in particular in the 'adiabatic regime' of large band gaps, while attractive interactions suppress Zener tunneling. Strong interactions cause a dynamical instability and thus a rapid depletion of the condensate mode. However, the mechanism of dynamical instability is significantly different: In the repulsive case, instability sets in at the edge of the Brillouin zone and is intimately related to the occurrence of looped Bloch bands. A condensate with attractive interactions is unstable already in the center of the Brillouin zone, leading to a collapse and explosion of the condensate.

On longer timescales, the interplay of Bloch oscillations and Landau-Zener tunneling leads to a complex dynamics due to the interference of the contributions in the two minibands. A quantitative analysis of this effects has been given, which also shows the applicability of Bloch-Zener oscillations in matter wave interferometry. A remarkable dynamics is also observed if transitions between the bands are not induced by a static external field, but by a periodic driving which leaves the quasimomentum unchanged. Because of the different curvature of the minibands, the matter waves in the two minibands move into opposite directions. The interference of the two contributions then leads to a dynamics which is comparable to the *Zitterbewegung* of a Dirac spinor.

Acknowledgments

This work has been supported by the German Research Foundation (DFG) through the research fellowship program (grant no WI 3415/1-1) and the Graduiertenkolleg 792 as well as the Studienstiftung des deutschen Volkes. We thank M. Weitz, T. Salger and M. Wubs for inspiring discussions.

-
- [1] F. Bloch, Z. Phys. **52**, 555 (1928).
 - [2] M. Ben Dahan, E. Peik, J. Reichel, Y. Castin, and C. Salomon, Phys. Rev. Lett. **76**, 4508 (1996).
 - [3] L. D. Landau, Phys. Z. Sowjetunion **2**, 46 (1932).
 - [4] C. Zener, Proc. R. Soc. London **137**, 696 (1932).
 - [5] E. Majorana, Nuovo Cimento **9**, 43 (1932).
 - [6] E. C. G. Stückelberg, Helv. Phys. Acta **5**, 369 (1932).
 - [7] A. J. Leggett, Rev. Mod. Phys. **73**, 307 (2001).
 - [8] O. Morsch and M. K. Oberthaler, Rev. Mod. Phys. **78**, 179 (2006).
 - [9] A. Görlitz, T. Kinoshita, T. W. Hänsch, and A. Hemmerich, Phys. Rev. A **64**, 011401(R) (2001).
 - [10] S. Fölling, S. Trotzky, P. Cheinet, M. Feld, R. Saers, A. Widera, T. Mueller, and I. Bloch, Nature **448**, 1029

- (2007).
- [11] G. Ritt, C. Geckeler, T. Salger, G. Cennini, and M. Weitz, *Phys. Rev. A* **74**, 063622 (2006),
 - [12] T. Salger, C. Geckeler, S. Kling, and M. Weitz, *Phys. Rev. Lett.* **99**, 190405 (2007).
 - [13] T. Salger, G. Ritt, C. Geckeler, S. Kling, and M. Weitz, *Phys. Rev. A* **79**, 011605(R) (2009).
 - [14] T. Salger, S. Kling, T. Hecking, C. Geckeler, L. Morales-Molina, and M. Weitz, *Science* **326**, 1241 (2009).
 - [15] S. Kling, T. Salger, C. Grossert, and M. Weitz, *Phys. Rev. Lett.* **105**, 215301 (2010)
 - [16] B. Wu and Q. Niu, *Phys. Rev. A* **61**, 023402 (2000).
 - [17] O. Zobay and B. M. Garraway, *Phys. Rev. A* **61**, 033603 (2000).
 - [18] Jie Liu, Libin Fu, Bi-Yiao Ou, Shi-Gang Chen, Dae-Il Choi, Biao Wu, and Qian Niu, *Phys. Rev. A* **66** 023404 (2002).
 - [19] E. M. Graefe, H. J. Korsch, and D. Witthaut, *Phys. Rev. A* **73**, 013617 (2006).
 - [20] B. P. Anderson and M. A. Kasevich, *Science* **282**, 1686 (1998).
 - [21] M. Jona-Lasinio, O. Morsch, M. Cristiani, N. Malossi, J. H. Müller, E. Courtade, M. Anderlini, and E. Arimondo, *Phys. Rev. Lett.* **91**, 230406 (2003).
 - [22] L. Fallani, L. De Sarlo, J. E. Lye, M. Modugno, R. Saers, C. Fort, and M. Inguscio, *Phys. Rev. Lett.* **93**, 140406 (2004).
 - [23] C. Sias, A. Zenesini, H. Lignier, S. Wimberger, D. Ciampini, O. Morsch, and E. Arimondo, *Phys. Rev. Lett.* **98**, 120403 (2007).
 - [24] A. Zenesini, H. Lignier, G. Tayebirad, J. Radogostowicz, D. Ciampini, R. Mannella, S. Wimberger, O. Morsch, and E. Arimondo, *Phys. Rev. Lett.* **103**, 090403 (2009).
 - [25] D. Witthaut, E. M. Graefe, and H. J. Korsch, *Phys. Rev. A* **73**, 063609 (2006).
 - [26] Biao Wu and Jie Liu, *Phys. Rev. Lett.* **96**, 020405 (2006).
 - [27] F. Trimborn, D. Witthaut, V. Kegel, and H. J. Korsch, *New J. Phys.* **12**, 053010 (2010).
 - [28] B. M. Breid, D. Witthaut, H. J. Korsch, *New J. Phys.* **8**, 110 (2006).
 - [29] B. M. Breid, D. Witthaut, H. J. Korsch, *New J. Phys.* **9**, 62 (2007).
 - [30] D. Jaksch, C. Bruder, J. I. Cirac, C. W. Gardiner, and P. Zoller, *Phys. Rev. Lett.* **81**, 3108 (1998).
 - [31] A. Vardi and J. R. Anglin, *Phys. Rev. Lett.* **86**, 568 (2001).
 - [32] J. R. Anglin and A. Vardi, *Phys. Rev. A* **64**, 013605 (2001).
 - [33] I. Tikhononkov, J. R. Anglin and A. Vardi, *Phys. Rev. A* **75**, 013613 (2007).
 - [34] D. Witthaut, K. Rapedius, and H. J. Korsch, *J. Nonlin. Math. Phys.* **16**, 207 (2009).
 - [35] B. Wu and Q. Niu, *New J. Phys.* **5**, 104 (2003).
 - [36] Y. Castin and R. Dum, *Phys. Rev. A* **57**, 3008 (1998).
 - [37] F. Trimborn, D. Witthaut, and H. J. Korsch, *Phys. Rev. A* **77**, 043631 (2008).
 - [38] F. Trimborn, D. Witthaut, and H. J. Korsch, *Phys. Rev. A* **79**, 013608 (2009).
 - [39] A. R. Kolovsky, H. J. Korsch, and E.-M. Graefe, *Phys. Rev. A* **80**, 023617 (2009).
 - [40] D. Witthaut, M. Werder, S. Mossmann, and H. J. Korsch, *Phys. Rev. E* **71**, 036625 (2005).
 - [41] M. Gustavsson, E. Haller, M. J. Mark, J. G. Danzl, G. Rojas-Kopeinig, and H.-C. Nägerl, *Phys. Rev. Lett.* **100**, 080404 (2008).
 - [42] S. Longhi, *Phys. Rev. B* **81**, 075102 (2010).
 - [43] S. Longhi, *Phys. Rev. A* **81**, 022118 (2010).